ACS APPLIED MATERIALS & INTERFACES

Research Article

www.acsami.org

Nanotextured Polymer Substrate for Flexible and Mechanically Robust Metal Electrodes by Nanoimprint Lithography

Hyeonjin Eom,[†] Jae-Han Kim,[‡] Junyoung Hur,[‡] Taek-Soo Kim,[‡,§] Sang-Keun Sung,[∥] Jun-Hyuk Choi,[∥] Eungsug Lee,[∥] Jun-Ho Jeong,*[,∥] and Inkyu Park*[,‡,§]

[†]Surface Technology R&D Group, Korea Institute of Industrial Technology (KITECH), Incheon 406-840, Korea

[‡]Department of Mechanical Engineering and [§]KI for the NanoCentury, Korea Advanced Institute of Science and Technology (KAIST), Daejeon 305-701, Korea

[∥]Department of Nano Manufacturing Technology, Korea Institute of Machinery and Materials (KIMM), Daejeon 305-343, Korea

Supporting Information

ABSTRACT: Metal thin film electrodes on flexible polymer substrates are inherently unstable against humidity and mechanical stresses because of their poor adhesion properties. We introduce a novel approach for improving the adhesion characteristics of metal−polymer interface based on the nanostructuring of the polymer substrate by using nanoimprint lithography. The adhesion characteristics of metal−polymer interface were measured by accelerated test, cyclic bending test and double cantilever beam (DCB) test. The interface of Au/Ti dual layer thin film and nanoimprinted PMMA substrate shows over 2.03 and 1.95 times higher adhesion energy (G_c) than that of Au/Ti dual layer thin film and plane PMMA substrate in air and wet environments, respectively. The adhesion energy between metal thin film and polymer substrate was dramatically improved by the increased surface roughness and mechanical interlocking effect of numerous nanoscale anchors at the edges of nanoimprinted surface, which was verified by both experiment and numerical analysis.

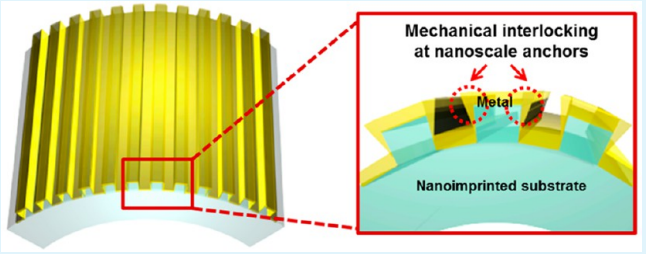

KEYWORDS: *surface adhesion, nanotextured substrate, nanoimprint lithography, metal−polymer interface, flexible substrate*

INTRODUCTION

Recently, various flexible electronic devices such as flexible sensors,[1−3] solar cells,[4] batteries,[5] and displays[6] are being actively developed. Accordingly, conductive electrodes based on metal thin films,[7,8] silver nanowires (AgNWs),[9,10] carbon nanotubes (CNTs),[11] and graphene[12,13] are being widely used in flexible electronic devices. Among these materials, metal thin films fabricated by printing or vacuum deposition processes are still more common due to their simplicity, high electrical conductivity and easy patterning methods.[7,8] However, electrical and mechanical failures often occur at the interface between metal thin film and flexible polymer substrate[14,15] under external stresses such as repeated bending or stretching. Moreover, metal thin films can be easily delaminated in wet environments because of the moisture-assisted adhesion weakening.[16−18] This becomes a significant problem during the liquid-phase synthesis of functional materials, solution-phase coating on the electrodes, or device operation in wet environments. Moreover, mechanical failure of conductive electrodes can be significant in wearable devices exposed to chemically reactive conditions (e.g., human sweat, breath, and external humidity).[19,20] Therefore, the enhancement of the adhesion energy between metal thin film and polymer substrates is essential to facilitate the flexible and stretchable microelectronic devices with high mechanical robustness.

To overcome the weak interfacial adhesion between metal thin film and polymer substrates, researchers have previously investiagted various methods. For instance, O_2 plasma treatment was found to provide higher interfacial adhesion between metal thin film and polymer substrate as compared to bare polymer substrate. The reasons include increased chemical binding energy,[21,22] cross-linked surface produced by the recombination of polymer radicals[21] and larger contact area with increased surface roughness.[23] Titanium (Ti) or chromium (Cr) thin film also has been used as an adhesive interlayer between metal and polymer substrate since they provide higher chemical bonding energy.[24−26] However, the adhesion of the metal−polymer interface assisted by these methods is still insufficient to prevent the mechanical failure of metal thin films in real-life applications of various flexible electronic devices.[14]

Herein, we propose a novel approach to dramatically improve the interfacial adhesion between metal thin film and polymer substrate by using periodic nanotextures of polymer substrates via nanoimprint lithography. Nanoimprinted substrate provides not only larger surface area and roughness but

Received: July 21, 2015
Accepted: October 26, 2015
Published: October 26, 2015

DOI: 10.1021/acsami.5b06631
ACS Appl. Mater. Interfaces 2015, 7, 25171−25179

Scheme 1. Enhancement of Surface Adhesion of Metal Thin Films on Polymer Substrate by Nanotexturing of Substrate via Nanoimprint Lithography: (a) Formation of Nanoline Array Pattern on Polymer Substrate by Nanoimprint Lithography, (b) Deposition of Metal Thin Film on the Nanoimprinted Polymer Substrate by Evaporation Process, (c) Illustration of Enhanced Adhesion of Metal Thin Film on Nanoimprinted Polymer Substrate (Inset: Schematic of Mechanical Interlocking Effect by Nanoscale Anchors)

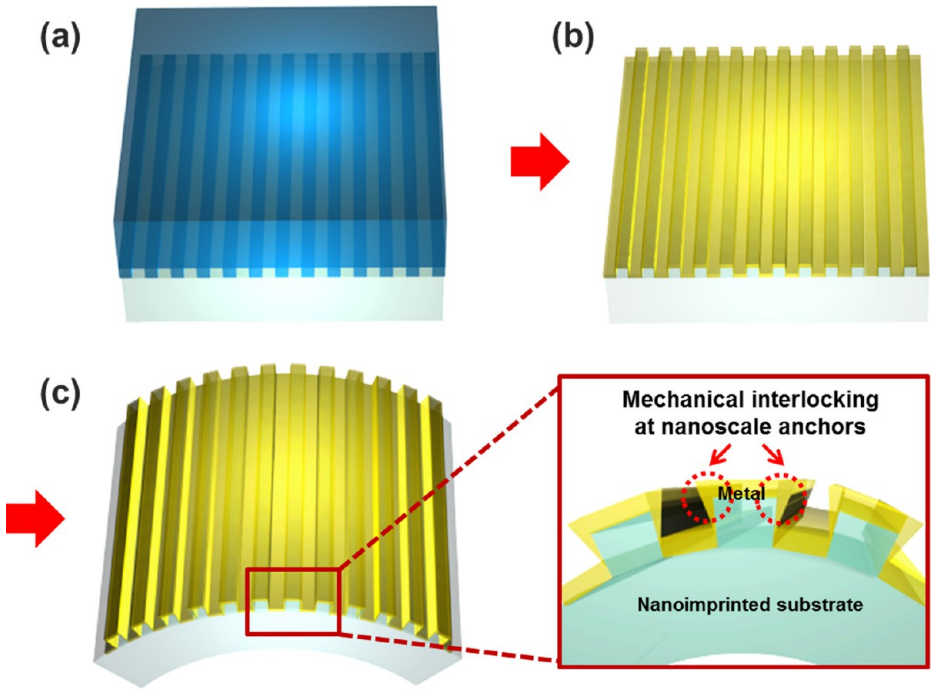

also mechanical interlocking with metal thin film. Specifically, an enhanced adhesion characteristics of the metal–polymer interface is obtained by fabricating the nanoimprinted structures on the polymer surface (Scheme 1). The nanoimprinted polymer substrate presents an increased surface roughness with rectangular wave patterns throughout the entire substrate, which provide highly increased contact area for the deposited metal thin film, which enhance the mechanical interlocking between the metal thin film and substrate. This contributes to the improved mechanical durability of the flexible devices by preventing the mechanical failure of metal thin films from harsh operating conditions such as repeated bending and high moisture.

EXPERIMENTAL SECTION

Fabrication of Metal Thin Films on Bare and Nanoimprinted Polymer Substrates. We have used the interface between gold (Au) thin film and poly(methyl methacrylate) (PMMA) substrate as the model system to demonstrate our idea. A commercial PMMA film (SKYSUN Corp.) was thermally imprinted with a nanoimprinting mold composed of periodic line array patterns (line width = 200 nm and pitch = 400 nm) under a pressure of 30 bar at 150 °C for 5 min. After the sample was cooled down to room temperature (25 °C) and mold was detached, two types of metal thin films were deposited for the experimental tests: Au single layer thin film (200 nm thick Au layer) and Au/Ti dual layer thin film (200 nm/20 nm thick Au/Ti films) were deposited on the nanoimprinted substrate by using thermal evaporation. Au/Ti dual layer thin film was also fabricated on bare PMMA substrate and O_2 plasma-treated PMMA substrate by thermal evaporation for comparison with the nanoimprinted PMMA substrate. The O_2 plasma-treated PMMA film was formed by O_2 plasma process (100 W, 30 min) with O_2 plasma treatment system (Femto Science Inc., Cute model). It has been previously researched that the physical vapor deposition of metal thin film can cause the embedding of atoms or the change of surface properties of polymer substrate, and therefore the process condition can affect the durability of deposited metal thin film.[27,28] However, since we used the same evaporation condition (evaporation rate = 10 Å/s) with cooling system (PMMA substrates are attached on the cooling plate), we will focus only on the effect of substrate geometry in this work.

Surface and Mechanical Characterization. The surface morphologies and cross-sectional images of the samples were investigated by using a scanning electron microscope (SEM, XL30SFEG, Philips Corporation) and scanning probe microscope (SPM, XE-100, Park Systems). In order to evaluate the interfacial adhesion characteristics between metal thin film and polymer substrate, accelerated life test (in 80 °C deionized (DI) water for 4 h) and cyclic bending test (10 000 bending/relaxation cycles from a flat state ($\rho = \infty$) to a bent state (ρ = 1 cm) in ambient air condition were carried out. The change of sheet resistance was measured by four probe measurement system (FPP-2400, Dasol Engineering).

The adhesion energy between the metal thin film and various types of PMMA substrates (i.e., bare, O_2 plasma-treated and nanoimprinted) was measured by double cantilever beam (DCB) tests[29,30] in air or water bath at room temperature. In this work, accelerated tests, cyclic bending tests and double cantilever beam (DCB) tests were conducted in air or water to investigate the adhesion properties of metal–polymer interfaces. It should be noted that the observations in air or water would not be valid for some of the polymer–metal interfaces where harsh environmental conditions such as corrosion would play a major role. However, our investigation will be meaningful for many applications in which conductive electrodes are directly exposed to the air or immersed in water with low ionic concentrations.

RESULTS AND DISCUSSION

Figure 1a.1–c.1 shows the surface morphologies of bare PMMA substrate, O_2 plasma-treated PMMA substrate and nanoimprinted PMMA substrate, respectively, characterized by an atomic force microscopy (AFM). The root-mean-square surface roughness (R_q), peak-to-valley roughness (R_{pv}), and

DOI: 10.1021/acsami.5b06631
ACS Appl. Mater. Interfaces 2015, 7, 25171–25179

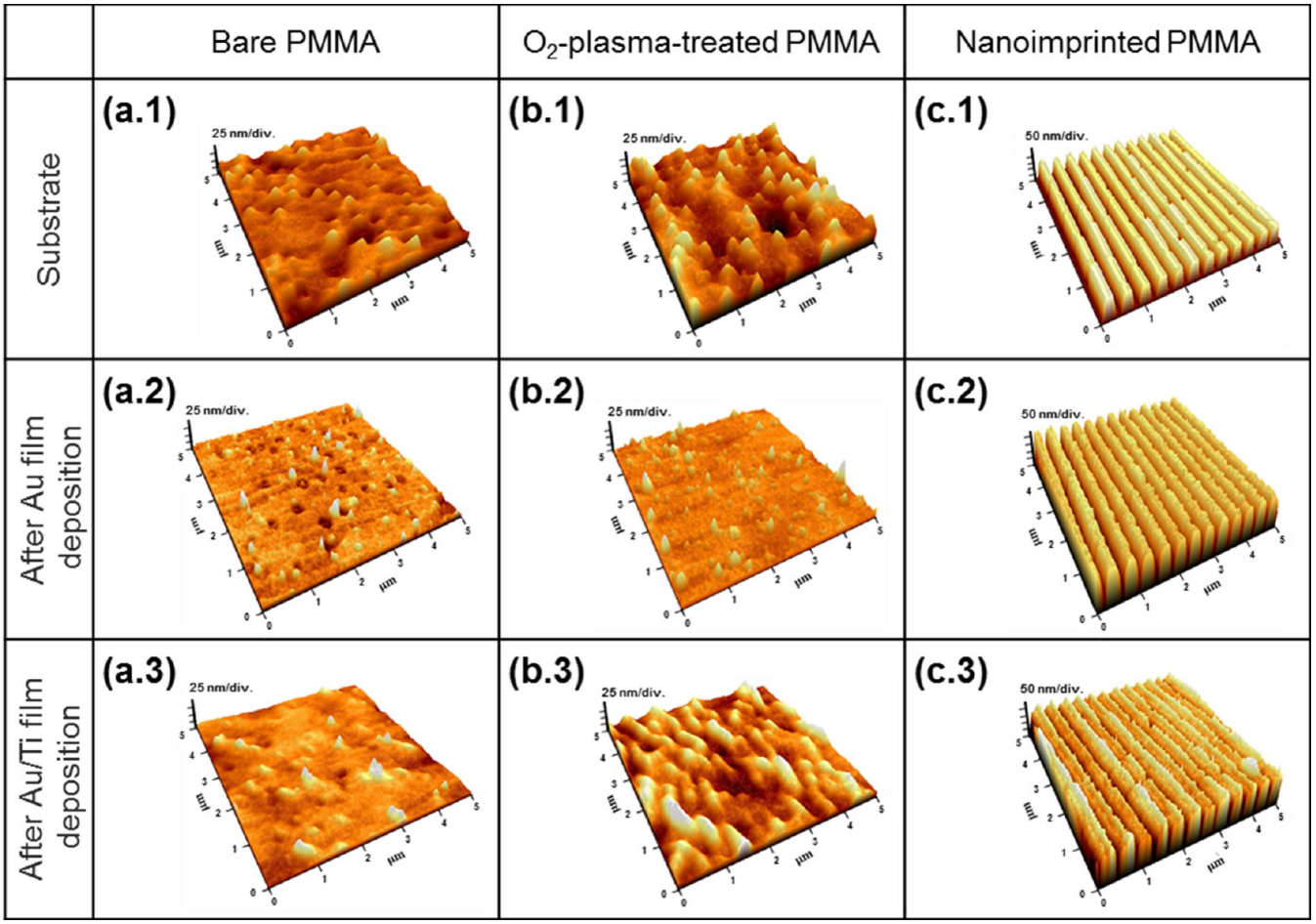

Figure 1. Surface morphologies of samples by scanning probe microscopy: (a.1) bare PMMA substrate, (b.1) O_2 plasma-treated PMMA substrate, and (c.1) nanoimprinted PMMA substrate; Au(200 nm) thin film deposited on (a.2) bare PMMA, (b.2) O_2 plasma-treated PMMA, and (c.2) nanoimprinted PMMA substrates, respectively; Au (200 nm)/Ti (20 nm) dual layer thin film deposited on (a.3) bare PMMA, (b.3) O_2 plasma-treated PMMA, and (c.3) nanoimprinted PMMA substrates, respectively.

average roughness (R_a) values for all samples are summarized in Table 1. The bare PMMA substrate shows a smooth surface

Table 1. Surface Roughness of Bare PMMA, O_2 Plasma-Treated PMMA and Nanoimprinted PMMA Substrates Measured by Scanning Probe Microscopy (R_q = root mean square roughness, R_{pv} = peak-to-valley, roughness and R_a = average roughness)

surface roughness (units)	R_q (nm)	R_{pv} (nm)	R_a (nm)
bare PMMA substrate	5.7	50.8	4.2
O_2 plasma-treated PMMA substrate	13.0	102.6	9.9
nanoimprinted PMMA substrate	15.8	131.1	11.1

with R_q = 5.7 nm, R_{pv} = 50.8 nm, and R_a = 4.2 nm. After the O_2 plasma treatment, the surface roughness of PMMA substrate increased to R_q = 13.0 nm, R_{pv} = 102.6 nm, and R_a = 9.9 nm, respectively. The surface roughening can be attributed to the degradation of PMMA chains by O_2 plasma treatment.[31,32] The nanoimprinted PMMA substrate shows a periodic line array of rectangular wave patterns with width = 197.4 nm, pitch = 406.2 nm, and height = 131.1 nm, and measured roughness are R_q = 15.8 nm, R_{pv} = 131.1 nm. The height of nanoimprinted pattern is lower than that of nanoimprint stamp (~200 nm) because of insufficient pressure and process time (30 bar, 5 min). However, uniform and periodic nanolines of rectangular patterns were fabricated on the substrate. After the deposition of metal thin film (Au or Au/Ti) by the thermal evaporation on each sample, the surfaces of samples were maintained with similar morphologies because of uniform and directional deposition during the thermal evaporation process (Figure 1c.1−c.3).

The mechanical robustness of metal thin film on different substrates was first evaluated by observing the surface morphologies and measuring the sheet resistances of metal thin films after the accelerated test (in 80 °C DI water for 4 h) and cyclic bending test (10,000 cycles with curvature radius (ρ) of 1 cm), as shown in Figures 2, 3, and 4. The optical images of Au and Au/Ti thin films deposited on bare PMMA substrate, O_2 plasma-treated PMMA substrate and nanoimprinted PMMA substrate after the accelerated test are shown in Figure 2a-2, b-2, c-2, and d-2 (Au single-layer thin film) and Figure 3a-2, b-2, c-2, and d-2 (Au/Ti dual layer thin film), respectively. Both Au and Au/Ti thin films on bare PMMA substrate and O_2 plasma-treated PMMA substrate show some bubble shaped islands by the delamination of metal thin films from the polymer substrate due to the moisture-assisted crack growth at metal−polymer interface.[16] (Figures 2a-b.2 and 3a-b.2). On the contrary, both Au film and Au/Ti film on nanoimprinted substrate maintained their surface morphologies without deformation or delamination after acceleration test due to the strong adhesion

DOI: 10.1021/acsami.5b06631
ACS Appl. Mater. Interfaces 2015, 7, 25171−25179

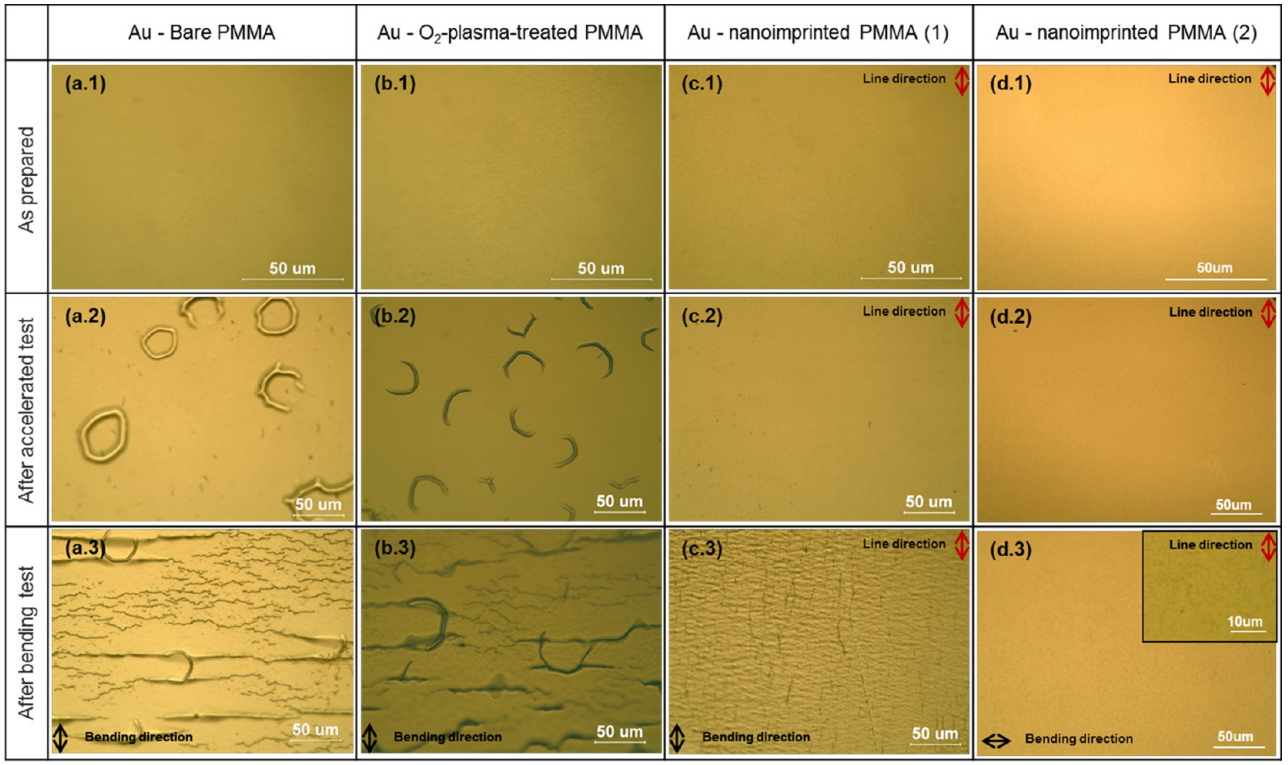

Figure 2. Optical images of surface of Au (200 nm) thin film on (a.1) bare PMMA, (b.1) O_2 plasma-treated PMMA, and (c.1, d.1) nanoimprinted PMMA substrates after thin film deposition and after (a.2−d.2) accelerated test and (a.3−d.3) bending test.

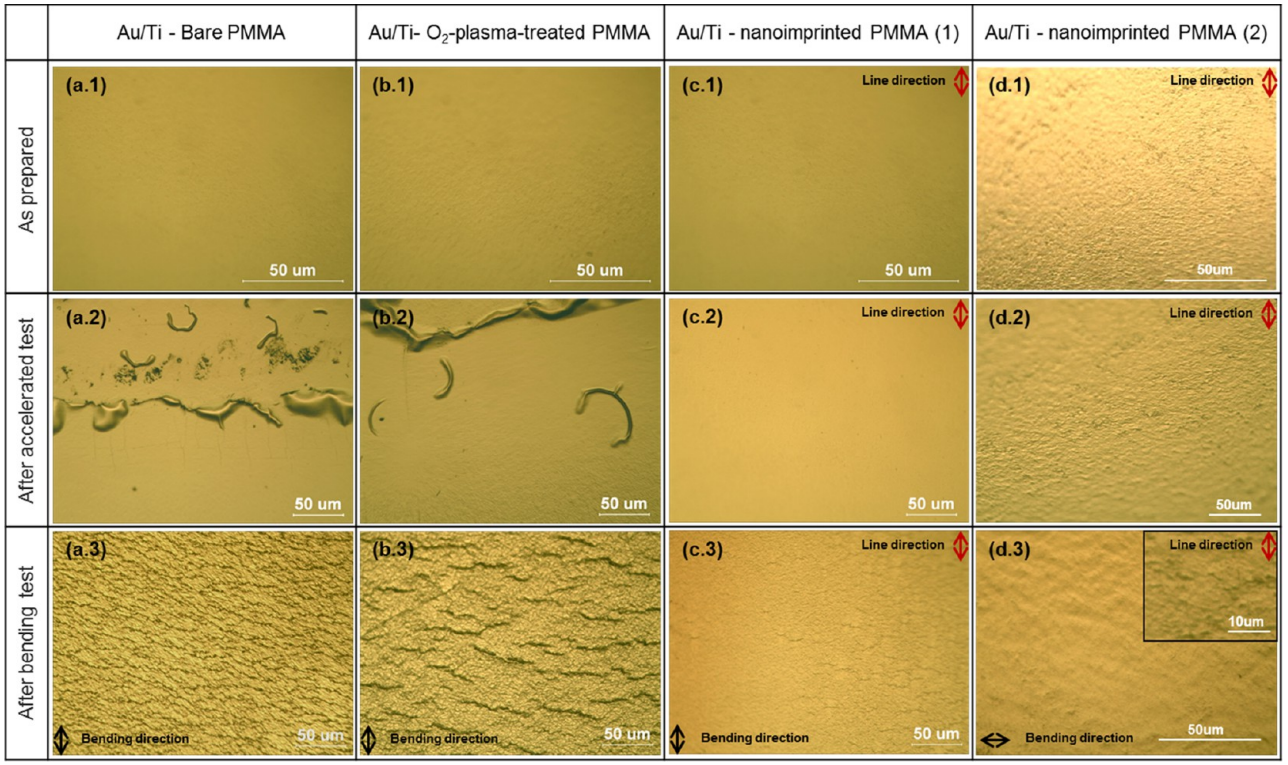

Figure 3. Optical images of surface of Au (200 nm)/Ti(20 nm) dual layer thin film on (a.1) bare PMMA, (b.1) O_2 plasma-treated PMMA, and (c.1, d.1) nanoimprinted PMMA substrates after thin film deposition and after (a.2−d.2) accelerated test and (a.3−d.3) bending test.

characteristics of the interface between metal thin film and nanoimprinted polymer substrate (Figures 2c-2 and 3c-2).

During cyclic bending test of the Au and Au/Ti thin films deposited on PMMA substrate, it appears that cracks were able to initiate either at the upper surface by tensile stress or at the thin film−substrate interface with tensile and shear stress state. After the cyclic bending test, Au thin films on a bare PMMA substrate and on a O_2 plasma-treated PMMA substrate show a

DOI: 10.1021/acsami.5b06631
ACS Appl. Mater. Interfaces 2015, 7, 25171−25179

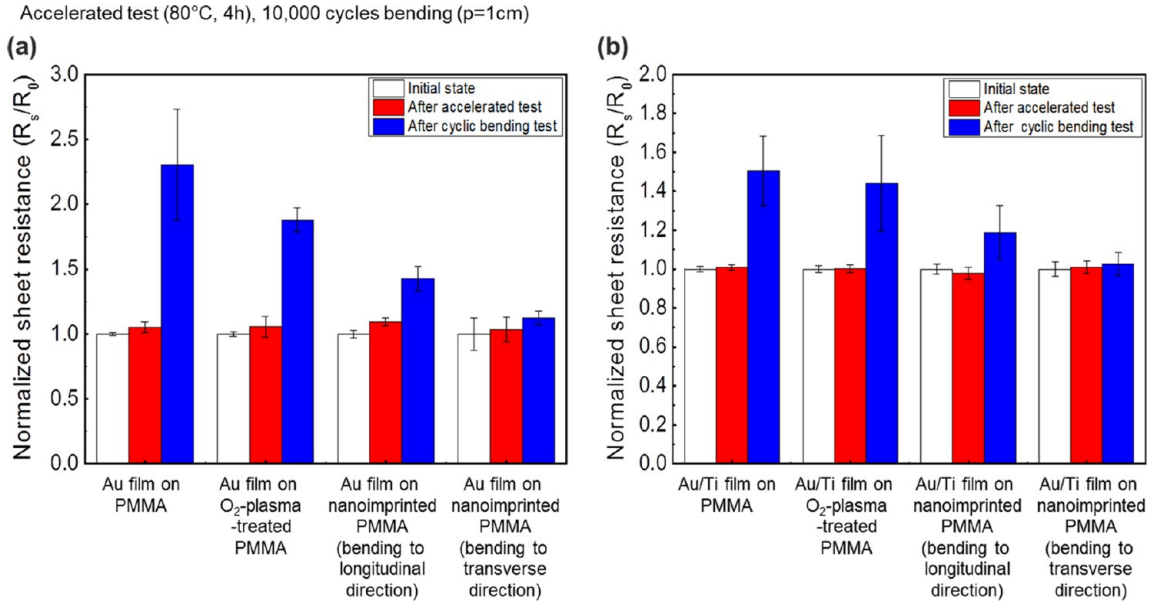

Figure 4. Relative changes of sheet resistances of metal thin films by accelerated and cyclic bending tests: (a) Au (200 nm) thin film on bare PMMA, O_2 plasma-treated PMMA and nanoimprinted PMMA substrates; (b) Au (200 nm)/Ti (20 nm) dual layer thin film on bare PMMA, O_2 plasma-treated PMMA, and nanoimprinted PMMA substrates before and after accelerated test and cyclic bending test.

large number of microcracks (average length: 52.4 (±14.7) μm and 62.2 (±25.7) μm, respectively). In contrast, the Au thin film on nanoimprinted PMMA substrate exhibits much higher mechanical robustness against cyclic bending. When it was bent in parallel with the direction of line pattern (i.e., axis of bending curvature in perpendicular direction to the line array), smaller cracks (average length: 18.8 (±6.1) μm) than those on the bare PMMA and O_2 plasma-treated PMMA substrate were formed (Figure 2a-3, b-3, c-3). The Au/Ti dual layer films on the bare PMMA and O_2 plasma-treated PMMA substrates also show a large number of microcracks (average length: 59.67(±16.62) and 63.22(±18.80) μm, respectively), whereas those on the nanoimprinted PMMA substrate bended in the longitudinal direction to the line pattern (i.e., axis of bending curvature in perpendicular direction to the line array) show much smaller cracks (average length: 15.35 (±5.77) μm) (see Figure 3a-3, b-3, c-3). Furthermore, almost no cracks were generated in both Au single layer and Au/Ti dual layer thin films on nanoimprinted PMMA substrate that were bent in the transverse direction to the line-pattern (i.e., axis of bending curvature in parallel with the line array) (see Figures 2d-3 and 3d-3) due to the larger interlocking effect at the edges of line-patterns to bending in the transverse direction than bending in the longitudinal direction. Because it is more difficult for the metal thin film to slide in the perpendicular direction to the line array of nanotextured surface, the crack propagation can be better hindered along this direction.

The sheet resistances of Au (200 nm) films on a bare PMMA substrate, O_2 plasma-treated PMMA substrate and nanoimprinted PMMA substrate were 122.66 (±1.66), 137.50 (±2.49), and 218.10 (±6.17) mΩ/sq (Figure 4a), respectively, and the sheet resistances of Au(200 nm)/Ti(20 nm) films on a bare PMMA substrate, O_2 plasma-treated PMMA substrate, and nanoimprinted PMMA substrate were 117.17 (±1.65), 125.66 (±2.44), and 229.20 (±5.83) mΩ/sq, respectively (Figure 4b). The initial sheet resistances of Au and Au/Ti thin films deposited on nanoimprinted PMMA substrate are higher than other samples because the metal thin films on some parts of the nanoimprinted surfaces (e.g., side walls or lower corners) are thinner than those on the horizontal surfaces because of the directional deposition of metal thin film during thermal evaporation process. After the accelerated test, the relative changes of sheet resistances ($R_s/R_{s,\ initial}$) of Au (200 nm) single-layer thin films on bare PMMA, O_2 plasma-treated PMMA, and nanoimprinted PMMA substrates were 1.05 (±0.04), 1.06 (±0.08), and 1.10 (±0.03). Also, the relative changes of sheet resistances ($R_s/R_{s,\ initial}$) of Au(200 nm)/Ti(20 nm) dual-layer thin films on bare PMMA, O_2 plasma-treated PMMA, and nanoimprinted PMMA substrates were 1.01 (±0.01), 1.00 (±0.02), and 0.98 (±0.03), respectively (Figure 4a). The changes of sheet resistances of metal thin films are insignificant after the accelerated test, which is not quite consistent with the surface morphology changes observed in Figures 2 and 3. The local delamination of metal thin films on bare PMMA and O_2 plasma-treated PMMA substrates does not significantly change the electrical resistance of thin films because they are still connected to the thin film and provide pathways for the electrical current. Although this could be insignificant in large-scale thin films, microscale delamination can lead to the complete failure of electrical interconnection in metal microelectrodes with microscale widths. The cyclic bending causes more severe degradation of electrical conductance of the metal thin films. After the cyclic bending test, relative changes of sheet resistances ($R_s/R_{s,\ initial}$) of Au thin films on bare, O_2 plasma-treated and nanoimprinted PMMA substrates were 2.30 (±0.43), 1.88 (±0.09), and 1.43 (±0.09) (Figure 4a). The relative changes of sheet resistances of Au/Ti dual layer films on bare, O_2 plasma-treated, and nanoimprinted PMMA substrates were 1.51 (±0.18), 1.44 (±0.25), and 1.19 (±0.14), respectively (Figure 4b). As mentioned above, the absolute sheet resistances of Au and Au/Ti thin films are lower on bare and O_2 plasma-treated PMMA substrates than on nanoimprinted PMMA substrate. However, the relative change of sheet resistances of metal thin films on bare PMMA and O_2 plasma-treated PMMA substrates are much higher than that of metal thin films on the

DOI: 10.1021/acsami.5b06631
ACS Appl. Mater. Interfaces 2015, 7, 25171−25179

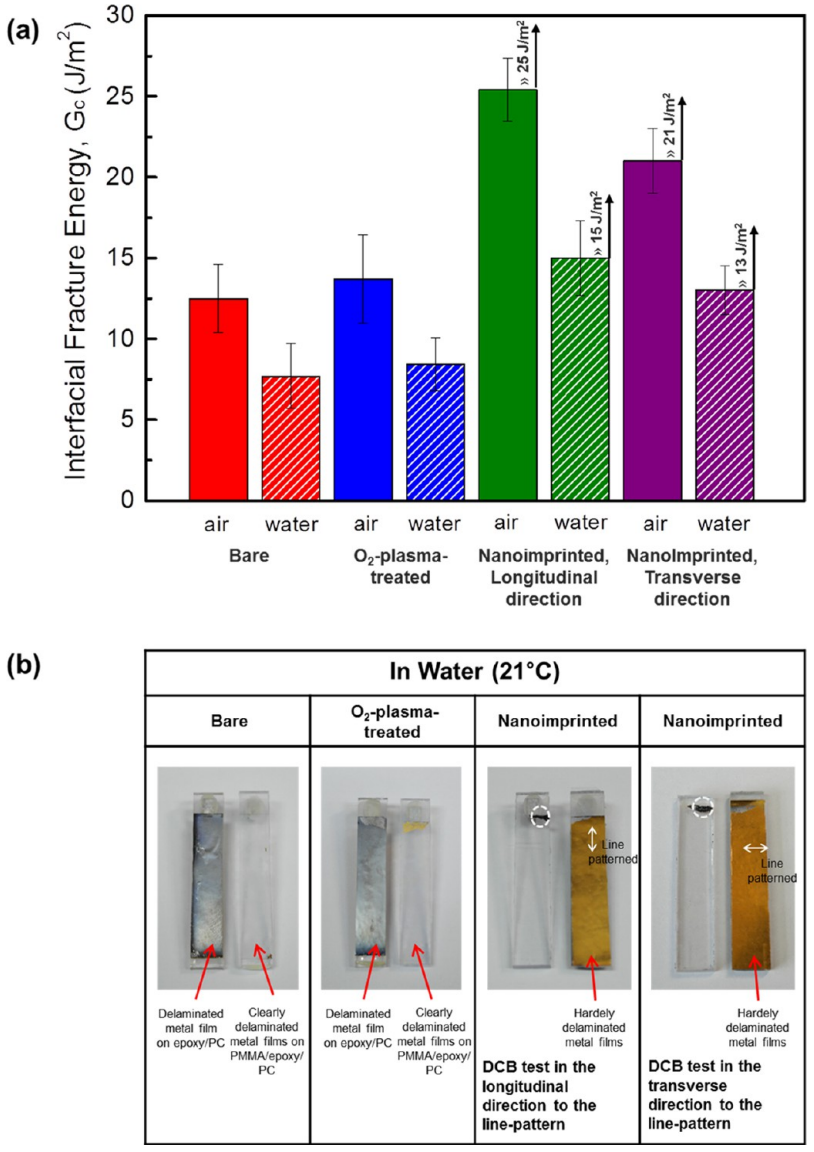

Figure 5. (a) Measured interfacial fracture energies of Au (200 nm)/Ti(20 nm) dual layer thin films on the bare PMMA, O_2 plasma-treated PMMA and nanoimprinted PMMA substrates in air and water; (b) delaminated surfaces of Au/Ti thin film on epoxy/Si substrate and delaminated surfaces from epoxy/Si substrate after DCB test in water.

nanoimprinted PMMA substrate. These larger changes are induced by greater amount of microcracks grown on bare and O_2 plasma-treated substrate as shown in Figures 2a-b.3 and 3a-b.3. In other words, larger averages, and standard deviations of sheet resistances after cyclic bending test were due to larger crack growth induced by the delamination of Au films from PMMA substrates because of lower adhesion forces at Au-PMMA interfaces for these samples. The sheet resistance changes of metal thin films on bare PMMA and O_2 plasma-treated PMMA substrates are higher than that of metal thin films on the nanoimprinted PMMA substrate. These higher electrical resistance changes are induced by large amount of microcracks shown in Figures 2a-b.3 and 3a-b.3. The plane substrate can slide and crack can propagate along the interface easily because of no interlocking effect along the interface. On the other hand, the metal thin films on nanoimprinted PMMA substrate bent in the longitudinal direction to the line pattern form less microcracks and thus result in smaller changes of the electrical resistance after the cyclic bending test (Figures 2c.3 and 3c.3). Moreover, in the case of metal thin films on nanoimprinted PMMA substrate bent in the transverse direction to the line pattern, the change of electrical resistance is much smaller than other cases. This result is consistent with the negligible microcracks on the metal thin film for these samples (Figures 2d.3 and 3d.3). These results prove that nanotexturing the PMMA substrate by nanoimprinting can be used for enhancing the adhesion of metal thin films on flexible polymer substrates to resist against harsh environments such as high temperature, moisture, and repeated bending.

To quantify the adhesion characteristics of the interface between metal thin film and polymer substrate, we measured interfacial adhesion energy (G_c) by the double cantilever beam (DCB) fracture mechanics test in air and water environments (details of the experimental procedure are explained in the Supporting Information). The DCB specimens were prepared by sandwiching the metal thin film/PMMA layer between polycarbonate (PC) substrates using an epoxy glue as shown in Figure S1a. The graph in Figure 5a summarizes G_c values of the

DOI: 10.1021/acsami.5b06631
ACS Appl. Mater. Interfaces 2015, 7, 25171−25179

Au/Ti on bare PMMA, O_2 plasma-treated PMMA and nanoimprinted PMMA substrates in air and water environments. The G_c value of Au-PMMA is higher than previously reported results because the metal films can be embedded into the surface of polymer substrate during the physical vapor deposition processes.[27,28] However, the embedding effect on the adhesion energy at the metal−PMMA interfaces would be same for all the samples because all metal thin films were deposited under the same evaporation condition (evaporation rate = 10 Å/s) and cooling condition (PMMA substrates were attached on the cooling plate). Therefore, geometry effect on the interfacial adhesion at the metal−polymer is focused in this work. First, the G_c values were calculated as 12.5 (±2.1), 13.7 (±2.7), and above 25.4 (±2.0) J/m^2 for the interfaces of Au/Ti−bare PMMA, Au/Ti layer−O_2 plasma-treated PMMA, and Au/Ti−nanoimprinted PMMA substrates in an air environment, respectively. The O_2 plasma-treated PMMA substrate shows slightly higher adhesion energy than that of bare PMMA substrate because the adhesion energy is increased by the oxygen functionality such as C−O bonds and C═O bonds generated after O_2 plasma treatment.[23,33,34] Moreover, the physical stiction of the plasma-treated substrate due to high surface roughness increases the physical adhesion energy to the Au/Ti dual layer thin film.[23] The nanoimprinted PMMA substrate shows greater adhesion energy than the O_2 plasma-treated PMMA substrate. The G_c values of Au/Ti dual-layer thin film−nanoimprinted PMMA substrate interface could not be measured, as the fracture occurred at the epoxy−Au/Ti dual-layer thin film interface because of significantly increased adhesion energy of Au/Ti dual layer thin film-nanoimprinted PMMA interface. On the contrary, Au/Ti dual layer thin films on bare PMMA and O_2 plasma-treated PMMA substrates were delaminated from the PMMA substrates after the DCB test. The measured G_c value of Au/Ti dual layer thin film-nanoimprinted PMMA in the transverse direction to the line-pattern in air was 21 J/m^2, but this correspond to the G_c for epoxy−Au/Ti dual layer thin film interface, as the fracture occurred at this interface because of higher adhesion energy of Au/Ti dual layer thin film−nanoimprinted PMMA substrate. The metal thin film could not be delaminated from the PMMA substrate in the transverse direction to the line pattern array during the DCB test. (Figure 5b and Figure S2) The G_c value measured in the longitudinal direction to the line-pattern is slightly higher than the G_c value measured in the transverse direction to the line-pattern, but these values correspond to the interface between epoxy layer and Au/Ti dual layer thin film. Therefore, it is difficult to compare G_c values of metal-nanoimprinted PMMA interface measured in the longitudinal and transverse directions to the line pattern array. The actual adhesion energy in the transverse direction to the line pattern array is expected to be larger than that in the longitudinal direction because of stronger interlocking effect of nanotextures in this direction (Figures 2c-d and 3c-d). The high adhesion energy of the Au/Ti- nanoimprinted PMMA interface can be mainly attributed to the significantly enhanced mechanical interlocking[33,35,36] and sticking effect induced by contact geometry of the nanoimprinted PMMA surface.

As mentioned above, when nanoimprinted PMMA substrates are mechanically bent, upper surface of metal thin film is under tensile stress and the metal−polymer interface is under both tensile and shear stress. In the case of longitudinal bending direction, nanopatterned surface cannot behave as an efficient mechanical obstacle. Thus, more microcracks can be propagated at the surface of metal films under mechanical loading. However, if bending occurrs in the transverse direction, more efficient mechanical interlocking at the interface prevents the failure at interfaces, which causes higher fracture toughness of metal film and less propagation of microcracks. Therefore, the actual adhesion energy in the transverse direction to the line pattern is expected to be much larger than that in the longitudinal direction

Different adhesion energies (G_c) for various PMMA substrates in the water environment show similar tendency as in the air environment except that their absolute values are lower. The G_c values of Au/Ti dual layer thin film are 7.7 (±2.0), 8.4 (±1.7), and above 15 (±2.3) J/m^2 for bare, O_2 plasma-treated, and nanoimprinted PMMA substrates in the water environment, respectively (Figure 5). All the adhesion energies of the metal thin film-PMMA substrate interface are lower in water than in air because the moisture lowers the crack driving force required for the crack growth.[16] In the moist environment, deboning of metal thin films can easily occur below the adhesion energy, G_c, and this is mainly attributed to the stress accelerated chemical reactions between environmental species and strained bonds at the crack front.[16,30] Similarly to the experiment in air environment, the real adhesion energies of the metal thin film−nanoimprinted PMMA interface are expected to be higher than the measured values because the detachment mostly occurred at the interface between Au/Ti dual layer film and epoxy/PS layer as shown in Figure 5b and Figure S2.

As explained above, the geometry of nanoimprinted PMMA substrate improves the mechanical interlocking and eventually results in the enhanced surface adhesion of metal thin films. We conducted a numerical simulation to investigate the geometrical effect of surface morphology of polymer substrate to the improvement of interfacial adhesion energy (see Figures S3 and S4 for detailed information on numerical analysis). Figure S4a, b shows the normal and shear stress distributions and evolution of crack between the Au thin film and PMMA substrate with periodic rectangular patterns (width and depth of trenches = 200 nm × 130 nm; pitch = 400 nm) during the interfacial separation. The pull-off forces for various surface morphologies such as rectangular, sinusoidal and plane surfaces were calculated by numerical simulation for comparison. Figure S4c compares the pull-off forces for different substrates. It is clearly shown that patterned interfaces have higher adhesion strength than the planar one. The rectangular patterned interface shows the highest pull-off force value, followed by the sinusoid patterned interface and planar surface. Increased energy dissipation by converting the direction of crack propagation from mode I (normal) to mode II (in-plane shear) in nanoimprinted substrate with numerous grooves leads to the enhancement of pull-off force.[37] From the experimental and numerical results, the rectangular patterns are advantageous to enhance the adhesion behavior because the width of the pattern is related to increasing the pull-off strength in mode I while the height controls the mode II loading. Therefore, rectangular patterned interface would show higher pull-off strength than other interfaces since the two modes are well-combined. Also, as the number of grooves is increased, each groove would function as an obstacle against the crack propagation by combination of mode I and mode II and thus the pull-off force is increased as shown in Figure S4c. Therefore, periodic nanoimprinted rectangular patterns can

DOI: 10.1021/acsami.5b06631
ACS Appl. Mater. Interfaces 2015, 7, 25171−25179

be considered as an ideal substrate structure with strong mechanical robustness for industrial applications.

CONCLUSIONS

In summary, we developed a novel method to improve the mechanical stability of the metal thin films on flexible polymer substrates by nanotexturing the substrate surface via direct nanoimprint lithography of substrate. We have found that the metal thin films deposited on the nanoimprinted polymer substrate exhibit much smaller change of electrical resistance as well as less mechanical failures such as delamination or crack propagation under accelerated moisture tests and cyclic bending tests, as compared to those deposited on the bare or O_2 plasma-treated polymer substrates. In addition, numerical analysis has proven that the periodic array of nanostructured metal−polymer interface with periodic patterns of rectangular cross-section enables strong mechanical interlocking effect, which improves the adhesion properties of metal−polymer interface. As a result, metal thin films deposited on nanoimprinted polymer substrate exhibited strong interfacial adhesion energy and this provided enhanced mechanical stabilities of the conductive electrode layer on the flexible substrate. Therefore, we expect that this approach can be widely used to improve the mechanical robustness of metal microelectrodes on flexible electronic devices and to prevent possible mechanical failures in moist and/or harsh environments. This technology would be also beneficial for skin-mountable devices that are in direct contact with human skin and under various mechanical loading, as well as for implantable biomedical devices that are exposed to wet and chemically harsh environments.

ASSOCIATED CONTENT

Supporting Information

The Supporting Information is available free of charge on the ACS Publications website at DOI: 10.1021/acsami.5b06631.

Numerical analysis of pull-off forces of nanoimprinted substrate and Figures S1−S4 (PDF)

AUTHOR INFORMATION

Corresponding Authors

*E-mail: jhjeong@kimm.re.kr.
*E-mail: inkyu@kaist.ac.kr.

Notes

The authors declare no competing financial interest.

ACKNOWLEDGMENTS

This research was supported by the Center for Advanced Meta-Materials (CAMM) funded by the Ministry of Science, ICT, and Future Planning as Global Frontier Project (CAMM 2014M3A6B3063707). This study was also supported by the Creative Research Program (ER150003) funded by the Ministry of Strategy and Finance and the grant (PNK4151) from Korea Institute of Materials (KIMS).

REFERENCES

(1) Yang, D.; Kim, D. H.; Ko, S. H.; Pisano, A. P.; Li, Z.; Park, I. Focused Energy Field (FEF) Method for the Localized Synthesis and Direct Integration of 1D Nanomaterials on Microelectronic Devices. *Adv. Mater.* **2015**, *27*, 1207−1215.

(2) Lim, M.; Kim, D.; Park, C.-O.; Lee, Y.; Han, S.-W.; Li, Z.; Williams, R. S.; Park, I. A New Route Towards Ultra-sensitive, Flexible Chemical Sensors: Metal Nanotubes by Wet-Chemical Synthesis along Sacrificial Nanowire Templates. *ACS Nano* **2011**, *6*, 598−608.

(3) Lee, J.; Kim, S.; Lee, J.; Yang, D.; Park, B. C.; Ryu, S.; Park, I. A Stretchable Strain Sensor Based on a Metal Nanoparticle Thin Film for Human Motion Detection. *Nanoscale* **2014**, *6*, 11932−11939.

(4) Yang, L. Q.; Zhang, T.; Zhou, H. X.; Price, S. C.; Wiley, B. J.; You, W. Solution-Processed Flexible Polymer Solar Cells with Silver Nanowire Electrodes. *ACS Appl. Mater. Interfaces* **2011**, *3*, 4075−4084.

(5) Chew, S. Y.; Ng, S. H.; Wang, J. Z.; Novak, P.; Krumeich, F.; Chou, S. L.; Chen, J.; Liu, H. K. Flexible Free-Standing Carbon Nanotube Films for Model Lithium-Ion Batteries. *Carbon* **2009**, *47*, 2976−2983.

(6) Liang, J. J.; Li, L.; Tong, K.; Ren, Z.; Hu, W.; Niu, X. F.; Chen, Y. S.; Pei, Q. B. Silver Nanowire Percolation Network Soldered with Graphene Oxide at Room Temperature and Its Application for Fully Stretchable Polymer Light-Emitting Diodes. *ACS Nano* **2014**, *8*, 1590−1600.

(7) Kim, S.; Lee, W. S.; Lee, J.; Park, I. *Nanotechnology* **2012**, *23*, 285301 Nanotechnology,.

(8) Sim, G.-D.; Won, S.; Jin, C.-Y.; Park, I.; Lee, S.-B.; Vlassak, J. J. Improving the Stretchability of As-Deposited Ag Coatings on PET Substrates Through Use of an Acrylic Primer. *J. Appl. Phys.* **2011**, *109*, 075311.

(9) Eom, H.; Lee, J.; Pichitpajongkit, A.; Amjadi, M.; Jeong, J. H.; Lee, E.; Lee, j. Y.; Park, I. Ag@Ni Core-shell Nanowire Network for Robust Transparent Electrodes against Oxidation and Sulfurization. *Small* **2014**, *10*, 4171−4181.

(10) Amjadi, M.; Pichitpajongkit, A.; Lee, S.; Ryu, S.; Park, I. Highly Stretchable and Sensitive Strain Sensor Based on Silver Nanowire-Elastomer Nanocomposite. *ACS Nano* **2014**, *8*, 5154−5163.

(11) Amjadi, M.; Yoon, Y. J.; Park, I. Ultra-Stretchable and Skin-Mountable Strain Sensors Using CNTs-Ecoflex Nanocomposite. *Nanotechnology* **2015**, *26*, 375501.

(12) Wang, X.; Zhi, L. J.; Mullen, K. Transparent, Conductive Graphene Electrodes for Dye-Sensitized Solar Cells. *Nano Lett.* **2008**, *8*, 323−327.

(13) Wu, J. B.; Becerril, H. A.; Bao, Z. N.; Liu, Z. F.; Chen, Y. S.; Peumans, P. Organic Solar Cells with Solution-Processed Graphene Transparent Electrodes. *Appl. Phys. Lett.* **2008**, *92*, 263302.

(14) Lee, I.; Kim, S.; Yun, J.; Park, I.; Kim, T.-S. Interfacial Toughening of Solution Processed Ag Nanoparticle Thin Films by Organic Residuals. *Nanotechnology* **2012**, *23*, 485704.

(15) Clarke, D. R.; Pompe, W. Critical Radius for Interface Separation of a Compressively Stressed Film from a Rough Surface. *Acta Mater.* **1999**, *47*, 1749−1756.

(16) Kook, S. Y.; Dauskardt, R. H. Moisture-Assisted Subcritical Debonding of a Polymer/Metal Interface. *J. Appl. Phys.* **2002**, *91*, 1293−1303.

(17) Dauskardt, R.; Lane, M.; Ma, Q.; Krishna, N. Adhesion and Debonding of Multi-Layer Thin Film Structures. *Eng. Fract. Mech.* **1998**, *61*, 141−162.

(18) Kim, J. H.; Nizami, A.; Hwangbo, Y.; Jang, B.; Lee, H. J.; Woo, C. S.; Hyun, S.; Kim, T. S. Tensile Testing of Ultra-Thin Films on Water Surface. *Nat. Commun.* **2013**, *4*, 2520.

(19) Elechiguerra, J. L.; Larios-Lopez, L.; Liu, C.; Garcia-Gutierrez, D.; Camacho-Bragado, A.; Yacaman, M. J. Corrosion at the Nanoscale: The Case of Silver Nanowires and Nanoparticles. *Chem. Mater.* **2005**, *17*, 6042−6052.

(20) Rathmell, A. R.; Nguyen, M.; Chi, M. F.; Wiley, B. J. Synthesis of Oxidation-Resistant Cupronickel Nanowires for Transparent Conducting Nanowire Networks. *Nano Lett.* **2012**, *12*, 3193−3199.

(21) Arefi, F.; Andre, V.; Montazerrahmati, P.; Amouroux, J. Plasma Polymerization and Surface-Treatment of Polymers. *Pure Appl. Chem.* **1992**, *64*, 715−723.

(22) Escaig, B. Binding Metals to Polymers - a Short Review of Basic Physical-Mechanisms. *J. Phys. IV* **1993**, *3*, 753−761.

(23) Lee, J. H.; Hwang, K. S.; Kim, T. S.; Seong, J. W.; Yoon, K. H.; Ahn, S. Y. Effect of Oxygen Plasma Treatment on Adhesion

DOI: 10.1021/acsami.5b06631
ACS Appl. Mater. Interfaces 2015, 7, 25171−25179

Improvement of Au Deposited on Pa-C Substrates. *J. Korean Phys. Soc.* **2004**, *44*, 1177−1181.
(24) Yu, J.; Song, J. Y.; Park, I. S. Analyses of the Practical Adhesion Strengths of the Metal/Polymer Interfaces in Electronic Packaging. *J. Electron. Mater.* **2002**, *31*, 1347−1352.
(25) Harman, G. G. *Wire Bonding in Microelectronics: Materials, Processes, Reliability, and Yield*, 2nd ed.; McGraw−Hill: New York, 1997; pp *xiv*.
(26) Pan, J. B.; Pafchek, R. M.; Judd, F. F.; Baxter, J. B. Effect of Chromium-Gold and Titanium-Titanium Nitride-Platinum-Gold Metallization on Wire/Ribbon Bondability. *IEEE Trans. Adv. Packag.* **2006**, *29*, 707−713.
(27) Schwartzkopf, M.; Santoro, G.; Brett, C. J.; Rothkirch, A.; Polonskyi, O.; Hinz, A.; Metwalli, E.; Yao, Y.; Strunskus, T.; Faupel, F.; Muller-Buschbaum, P.; Roth, S. V. Real-Time Monitoring of Morphology and Optical Properties During Sputter Deposition for Tailoring Metal-Polymer Interfaces. *ACS Appl. Mater. Interfaces* **2015**, *7*, 13547−13556.
(28) Bowden, N.; Brittain, S.; Evans, A. G.; Hutchinson, J. W.; Whitesides, G. M. Spontaneous Formation of Ordered Structures in Thin Films of Metals Supported on an Elastomeric Polymer. *Nature* **1998**, *393*, 146−149.
(29) Kanninen, M. F. Augmented Double Cantilever Beam Model for Studying Crack-Propagation and Arrest. *Int. J. Fract.* **1973**, *9*, 83−92.
(30) Lee, C. H.; Kim, J. H.; Zou, C. Y.; Cho, I. S.; Weisse, J. M.; Nemeth, W.; Wang, Q.; Van Duin, A. C. T.; Kim, T. S.; Zheng, X. L. Peel-and-Stick: Mechanism Study for Efficient Fabrication of Flexible/Transparent Thin-Film Electronics. *Sci. Rep.* **2013**, *3*, 2917.
(31) Schulz, U.; Munzert, P.; Kaiser, N. Surface Modification of Pmma by Dc Glow Discharge and Microwave Plasma Treatment for the Improvement of Coating Adhesion. *Surf. Coat. Technol.* **2001**, *142*, 507−511.
(32) Vourdas, N.; Tserepi, A.; Gogolides, E. Nanotextured Super-Hydrophobic Transparent Poly(Methyl Methacrylate) Surfaces Using High-Density Plasma Processing. *Nanotechnology* **2007**, *18*, 125304.
(33) Kim, S. H.; Na, S. W.; Lee, N. E.; Nam, Y. W.; Kim, Y. H. Effect of Surface Roughness on the Adhesion Properties of Cu/Cr Films on Polyimide Substrate Treated by Inductively Coupled Oxygen Plasma. *Surf. Coat. Technol.* **2005**, *200*, 2072−2079.
(34) Chai, J. N.; Lu, F. Z.; Li, B. M.; Kwok, D. Y. Wettability Interpretation of Oxygen Plasma Modified Poly(Methyl Methacrylate). *Langmuir* **2004**, *20*, 10919−10927.
(35) Cui, L. Y.; Ranade, A. N.; Matos, M. A.; Dubois, G.; Dauskardt, R. H. Improved Adhesion of Dense Silica Coatings on Polymers by Atmospheric Plasma Pretreatment. *ACS Appl. Mater. Interfaces* **2013**, *5*, 8495−8504.
(36) Shenton, M. J.; Lovell-Hoare, M. C.; Stevens, G. C. Adhesion Enhancement of Polymer Surfaces by Atmospheric Plasma Treatment. *J. Phys. D: Appl. Phys.* **2001**, *34*, 2754−2760.
(37) Lee, M. J.; Lim, J. M.; Lee, B. C. Finite Element Analysis of an Adhesive Joint Using the Cohesive Zone Model and Surface Pattern Design of Bonding Surfaces. *J. Adhes.* **2013**, *89*, 205−224.

DOI: 10.1021/acsami.5b06631
ACS Appl. Mater. Interfaces 2015, 7, 25171−25179